Nanoscale

Computational investigation on lipid bilayer disruption induced by amphiphilic Janus nanoparticles: combined effect of Janus balance and charged lipid concentration

Journal:	*Nanoscale*
Manuscript ID	NR-ART-01-2023-000403.R2
Article Type:	Paper
Date Submitted by the Author:	19-Aug-2023
Complete List of Authors:	Nguyen, Danh ; University of Wisconsin-Madison, Mechanical Engineering Wu, James; University of California Berkeley, Department of Molecular and Cell Biology Corrigan, Patrick ; University of Connecticut, Chemistry Li, Ying; University of Wisconsin-Madison, Mechanical Engineering; University of Wisconsin-Madison

ARTICLE

Computational investigation on lipid bilayer disruption induced by amphiphilic Janus nanoparticles: combined effect of Janus balance and charged lipid concentration

Received 00th January 20xx,
Accepted 00th January 20xx

DOI: 10.1039/x0xx00000x

Danh Nguyen,[a] James Wu,[b] Patrick Corrigan,[c] and Ying Li*[a]

Janus nanoparticles (NPs) with charged/hydrophobic compartments have garnered attention for their potential antimicrobial activity. These NPs have been shown to disrupt lipid bilayers in experimental studies, yet the underlying mechanisms of this disruption at the particle-membrane interface remain unclear. To address this knowledge gap, the present study conducts a computational investigation to systematically examine the disruption of lipid bilayers induced by amphiphilic Janus NPs. The focus of this study is on the combined effects of the hydrophobicity of the Janus NP, referred to as the Janus balance, defined as the ratio of hydrophilic to hydrophobic surface coverage, and the concentration of charged phospholipids on the interactions between Janus NPs and lipid bilayers. Computational simulations were conducted using a coarse-grained molecular dynamics (MD) approach. The results of these MD simulations reveal that while the area change of the bilayer increases monotonically with the Janus balance, the effect of charged lipid concentration in the membrane is not easy to be predicted. Specifically, it was found that the concentration of negatively charged lipids is directly proportional to the intensity of membrane disruption. Conversely, positively charged lipids have a negligible effect on membrane defects. This study provides molecular insights into the significant role of Janus balance in the disruption of lipid bilayers by Janus NPs and supports the selectivity of Janus NPs for negatively charged lipid membranes. Furthermore, the anisotropic properties of Janus NPs were found to play a crucial role in their ability to disrupt the membrane via the combination of hydrophobic and electrostatic interactions. This finding is validated by testing the current Janus NP design on a bacterial membrane-mimicking model. This computational study may serve as a foundation for further studies aimed at optimizing the properties of Janus NPs for specific antimicrobial applications.

Introduction

Nanoparticles (NPs) have been the subject of numerous studies investigating the role of their surface properties in interactions with biological membranes.[1] Recent research has demonstrated that cationic and anionic NPs can effectively disrupt the structure and function of biological membranes.[2-5] While previous studies have primarily focused on NPs with a uniform surface composition, recent attention has been directed toward NPs with heterogeneous arrangements of ligands, as they have been shown to interact with cell membranes more effectively.[6, 7] One type of heterogeneous NP that has gained particular interest is the Janus NP. These NPs are useful in a wide variety of applications, including optics, catalysis, drug delivery, bioimaging, and biosensing.[8-10] The unique conformation of the Janus NP makes it more effective in facilitating interfacial activity (i.e. adsorption/desorption) compared to homogenous particles.[11] Additionally, Janus NPs can carry a greater variety of cancer treatments than conventional core-shell particles.[8, 12] Recent studies have also suggested that Janus NPs with charged/hydrophobic compartments have the potential for antimicrobial activity, as they have been shown to disrupt lipid bilayers in experiments.[13] These findings indicate that Janus NPs may have promising applications in nanomedicine field, particularly in treating cancer, bacterial infection, and other diseases.

The mechanisms behind the disruption of lipid membranes induced by Janus NPs are not fully understood. A critical area of research is the impact of the hydrophobicity of Janus NPs and lipid membrane composition on particle-membrane interactions. Recently, Yu and co-workers conducted a quantitative investigation on the role of hydrophobicity in the interactions between Janus NPs and zwitterionic lipid membranes.[14] By adjusting the Janus balance, the authors established a quantitative relationship between the hydrophobicity of amphiphilic Janus NPs and their influence on lipid membranes. In a separate study, we investigated the effect of membrane lipid composition on Janus NP-membrane interactions.[15] We found that different lipid compositions of phospholipids and cholesterol can lead to various co-existence of liquid-ordered and liquid-disordered phases in the lipid bilayers. As a result, Janus NPs caused different disruptive

[a] Department of Mechanical Engineering, University of Wisconsin-Madison, Madison, WI 53706, USA.
[b] Department of Molecular and Cell Biology, University of California, Berkeley, CA 94720, USA.
[c] Department of Chemistry, University of Connecticut, Storrs, CT 06269, USA.
* Correspondence: Email: yli2562@wisc.edu
Electronic Supplementary Information (ESI) available: [details of any supplementary information available should be included here]. See DOI: 10.1039/x0xx00000x

behaviours towards these membranes in both experiments and simulations.[15]

In addition to cholesterol, the presence of negatively and positively charged phospholipids in lipid bilayers can accurately represent real-life biological membranes, leading to complex NP-membrane phenomena. Specifically, charged phospholipids are essential components in the cell membranes of living organisms, regulating the association of proteins with the plasma membrane.[16] Previous studies have shown that Janus NPs can generate defects in cationic and anionic lipid bilayers,[17] but the underlying mechanisms governing the interactions between Janus NPs and charged lipid membranes have yet to be thoroughly investigated. Some crucial areas of research include determining (1) if hydrophobic interactions are the primary driving force during the interaction between NPs and charged lipid bilayers and (2) if electrostatic interactions due to the presence of charged lipids assist or hinder membrane disruption. From an experimental perspective, it is widely accepted that hydrophobic interactions between ligands of Janus NPs and phospholipids in the membrane are key drivers of lipid extraction and membrane defect formation.[13, 18]

However, the concentration of charged lipids in the membrane could also impact membrane alteration. Despite some prior research in this area,[14, 17] there is a lack of systematic studies on the combined effect of Janus balance and membranes with varying charged lipid concentrations at the molecular scale. To address this knowledge gap, we aim to use molecular dynamics (MD) simulations to systematically study the combined effect of these parameters on Janus NP-membrane interactions. MD simulations are a powerful tool for extracting meaningful information that can be difficult to acquire through experimentation, such as the structural dynamics of biological molecules.[19, 20] Additionally, MD simulations allow for the exploration of a broader range of design parameters than experimentation, which is helpful for the discovery of novel antibiotics.[21] Furthermore, MD simulations can help reveal the molecular mechanisms underlying phenomena observed experimentally. For example, our previous research used MD simulations to effectively explain the stronger disruptive capability of Janus NPs towards the membrane of giant unilamellar vesicles (GUVs) compared to uniform particles,[18] and the domain-selective disruption and compression of phase-separated GUVs induced by Janus NPs.[15]

In this study, we employ coarse-grained MD simulations with the MARTINI force field[22] to systematically investigate how Janus NPs with varying Janus balances interact with charged membranes of different lipid compositions. To mimic the anisotropic characteristics of Janus NPs, we adopt the molecular model of Janus NP used in our previous studies.[15, 18] To vary the Janus balance, three different area densities of the hydrophilic and hydrophobic portions of the Janus NP will be used: 90/10, 80/20, and 50/50 ratios. Additionally, uniform amphiphilic NPs will be built with random distributions of hydrophilic beads and hydrophobic ligands as a control model to validate the role of the particle surface anisotropy.

To understand the pathway of the interaction between Janus NPs and lipid bilayers, we will perform a two-dimensional (2D) potential of mean force (PMF) calculation. The resulting free energy surface (FES) will indicate the preferred Janus NP orientations during interactions with lipid membranes. To evaluate the Janus NP-membrane interactions in different scenarios, we will extract and compare significant MD simulation results, including snapshots at varying time points during the interaction, projected area of lipid bilayers, lipid diffusivity, hydrophobic and electrostatic interaction energies, and the number of lipids extracted from the membranes over the course of simulations. Through these efforts, we aim to (1) establish a structure-activity relationship that explains how the hydrophobic/hydrophilic balance of Janus NPs can impact their membrane disruption activity, and (2) quantify the driving forces in the interactions between Janus NPs and charged membranes. These findings are expected to deepen our understanding of how lipid bilayers with various surface charges behave in the presence of Janus NPs, ultimately leading to improved nano-system design for real-life biological membrane applications.

To that end, this manuscript is organized as follows: **Section Computational Model and Methods** describes our MD simulation and computational approach; **Section Results and Discussion** includes five sub-sections: **Section Effect of Janus balance** provides the results and discussion related to how different Janus balances affect the stability and disruption of a pure phospholipid bilayer; **Section Effect of negatively charged lipid concentration** discusses the impact of anionic lipid concentration on the alteration of negatively charged membranes induced by Janus NPs; **Section Effect of positively charged lipid concentration** discusses the impact of cationic lipid concentration on the disruption of positively charged bilayers caused by Janus NPs; **Section Combination effects** summarizes the combined impact of the Janus balance and ionic lipid concentration on the NP-membrane interaction; and **Section Implement on bacterial membrane-mimicking model** discusses the potential of current Janus NP model to select for disrupting a negatively charged bacterial membranes. Finally, **Section Conclusions** summarizes our findings and provides conclusions regarding our computational investigation.

Computational Model and Methods

MARTINI force field descriptions

The Coarse-grained (CG) MD simulations are implemented using GROMACS version 2020.[23] Computational simulations of lipid membranes and Janus NPs using the CGMD approach are feasible on temporal and spatial scales that enable the capture of the fundamental interaction mechanisms. In this study, the MARTINI force field[24-30] will be employed to investigate the interactions between Janus NPs and various lipid bilayers. This force field is widely utilized for studying of NP–lipid membrane interactions[31-34] due to its ability to accurately reproduce the conformational, mechanical, and free energy characteristics of various lipids and molecular species in MD simulations.[28, 29, 35] In MARTINI force field, atoms are represented by CG beads, with

each bead representing up to four heavy atoms and is characterized as one of four types: polar (P), nonpolar (N), apolar (C), or charged (Q). From **Section Effect of Janus balance** to **Section Combination effects**, three lipid species, DOPC (1,2-dioleoyl-sn-glycero-3-phosphocholine), DOPA (anionic 1,2-dioleoyl-sn-glycero-3-phosphate), and DOTAP (cationic 1,2-dioleoyl-3-trimethylammonium-propane) are used in the planar lipid bilayer. The bead types used for each lipid are shown in **Fig. 1a**. The MARTINI force field for DOPC is implemented with the modified version,[15, 36] while DOPA and DOTAP are implemented with the standard MARTINI force field.[22] Additionally, a biologically accurate model of a membrane is simulated in **Section Implement on bacterial membrane-mimicking model**. This model consists of a mixture of lipopolysaccharide (LPS) and 1-palmitoyl-2-oleoyl-sn-glycero-3-phosphocholine (POPC). The CG beads of POPC are presented in **Fig. S7a** using a standard MARTINI force field.[22] The CG model and parameters of LPS (**Fig. S7b** and **Table S1)** are derived from CHARMM-GUI.[37]

Planar membrane model

The planar membrane models used in this study from **Section Effect of Janus balance** to **Section Combination effects** are constructed using the INSANE (INSert membraNE) script.[38] This tool allows for adjusting the size and composition of a MARTINI bilayer model and is used to create nine different membranes (**Table 1**) with varying compositions of DOPC, DOPA, and DOTAP. These membranes are composed of 1,568 CG lipids and 140,000 CG water and have a total system size of 23 × 23 × 36 nm^3 to accommodate a single Janus NP with a core diameter of 10 nm. In cases where uniform NP models are utilized, larger membranes (35 × 35 × 36 nm^3) are employed to eliminate the effect of boundary conditions.

The constructed membranes are then subjected to energy minimization using the steepest descent method (5,000 steps), followed by a successive isothermal–isobaric (NPT) equilibration simulation. The number of particles (N), constant pressure (P), and temperature (T) are all kept constant during the NPT simulation, which is performed for 30 ns with a timestep of 30 fs. This is followed by a 1.0 μs production simulation with a timestep of 30 fs. Reaction-field electrostatics are used with a Coulomb cut-off of 1.1 nm and dielectric constants of 15 or 0 within or beyond this cut-off distance, respectively. Lennard-Jones (LJ) interactions are cut off at 1.1 nm, shifting the potential energy to zero. Constant temperature is maintained at 310 K via separate coupling of the solvent (water) and lipid components to v-rescaling thermostat (relaxation time = 1.0 ps). Pressure is semi-isotropically coupled at 1.0 bar. The Berendsen scheme is used for the NPT equilibration with relaxation time and compressibility of 12.0 ps and 3 × 10^{-4} bar^{-1}, respectively. After equilibration, the Parrinello−Rahman barostat is used for the long production run.

In **Section Implement on bacterial membrane-mimicking model**, a bacterial-mimicking membrane model is constructed using CHARMM-GUI website.[37] The LPS/POPC membrane is initially generated using the MARTINI membrane builder tool within CHARMM-GUI, with a specific ratio of input lipids. The ratios of LPS to POPC used in the simulation are 5:95 (5% LPS) and 20:80 (20% LPS). The total number of CG lipids and waters in the LPS/POPC membranes are 1,170 and 140,000, respectively. The membrane is equilibrated by performing energy minimization (steepest descent, 5,000 steps) followed by subsequent NPT simulations with increasing time steps from 2.0 fs to 30 fs. A production simulation is then conducted for 1.0 μs with a timestep of 30 fs. The NPT and production runs parameters are similar to those used in the DOPC/DOPA (DOTAP) planar membrane modelling described above.

Table 1 List of planar lipid membranes used in this study.*

No.	DOPC [%]	DOPA (−) [%]	DOTAP (+) [%]	Properties
1	100	0	0	Hydrophobic
2	0	100	0	(−) Hydrophilic
3	0	0	100	(+) Hydrophilic
4	95	5	0	(−) Charged hydrophobic
5	90	10	0	(−) Charged hydrophobic
6	80	20	0	(−) Charged hydrophobic
7	95	0	5	(+) Charged hydrophobic
8	90	0	10	(+) Charged hydrophobic
9	80	0	20	(+) Charged hydrophobic

*Membrane dimension is 23 × 23 × 36 nm^3 when using anisotropic Janus NP models (JP 50/50, JP 80/20 and JP 90/10) or 35 × 35 × 36 nm^3 when using uniform particle models (JP WM) to mitigate the finite effects of planar membranes.

Models of Janus NP and MD simulations with planar membrane

The Janus NP model used in our simulation is adapted from our previous works.[15, 18] Briefly, the gold (Au) core of the Janus NP is constructed from a bulk face-centred cubic (FCC) lattice with a constant of 0.408 nm. The diameter of the Au core is chosen to be 10 nm, which is larger than the thickness of the lipid bilayer. The Au core is constructed with inert metal beads C5. The surface of the NP is divided into two distinct regions: a hydrophilic hemisphere and a hydrophobic hemisphere. The hydrophilic hemisphere is covered with positively charged hydrophilic beads (Qd) with an areal density of 2.5 nm^{-2}, while the hydrophobic hemisphere is covered with sulphur beads (N_0) with an area density of 4.7 nm^{-2}. Each N_0 bead is bonded with a hydrophobic alkyl chain represented by four C1 beads to mimic the octadecane carbon chain. The interactions between the Au beads in the core are treated with harmonic bond potentials using a force constant of 10,000 kJ mol^{-1} to ensure the rigidity of the core. The Au-Qd and Au-N_0 interactions are applied with a force constant of 6,400 kJ mol^{-1} with an equilibrium bond length of 0.24 nm. A harmonic bond potential force constant of 1,250 kJ mol^{-1} with an equilibrium bond length of 0.47 nm and a cosine angle potential of 180° with a force constant of 25 kJ mol^{-1} are applied to the bonds in the ligand. To reduce the computational cost, we kept the diameter of the NP core at 10 nm, which is about twice the thickness of a lipid bilayer. The Janus balance is represented by the hydrophilicity/ hydrophobicity ratio, which is varied in our simulations to study its effect on membrane disruption. The ratio used in this study are 90/10 (JP 90/10), 80/20 (JP 80/20), and 50/50 (JP 50/50). Additionally, a model of a uniform amphiphilic NP (JP WM) is established as a control model, with well-mixed hydrophilic beads and hydrophobic ligands (hydrophobicity of 50%), to compare its membrane disruptive effect with that of the anisotropic Janus NP model (JP 50/50).

The dynamics of a single Janus NP is subjected to a series of MD simulation steps. The simulation begins by positioning the NP 9.5 nm above the middle plane of the bilayer, as determined by the centre-of-mass (COM) distance. A steepest descent minimization procedure, consisting of 10,000 steps, is then applied to resolve any steric clashes. The system is subsequently equilibrated for 20 ns using an NPT ensemble. The production run is then performed for a total of 200 ns. In the case of multiple Janus NPs, as depicted in **Fig. S1**, four particles are placed near one another above the membrane to accelerate the cooperative effect of multiple NPs [15]. The simulation setup for these models follows the same procedure as the single Janus NP simulations for minimization and equilibration. However, the production run is extended to 1.0 μs to ensure sufficient simulation time for the cooperation of Janus NPs. The timestep for all Janus NP-membrane interaction simulations is set at 20 fs. Reaction-field electrostatics are used with a Coulomb cut-off of 1.4 nm and dielectric constants of 15 or 0 within or beyond this cut-off distance, respectively. The LJ force field is cut off at 1.4 nm, where the potential energy is shifted to zero. Constant temperature is maintained at 310 K via separate coupling of the solvent (water), lipids in the membrane and the Janus NP to v-rescaling thermostats with a relaxation time of 1.0 ps. In both equilibration and production stages, pressure is semi-isotropically coupled at 1.0 bar and controlled by the Berendsen barostat with a relaxation time of 12.0 ps and compressibility of 3×10^{-4} bar^{-1}.

2D potential mean force (PMF) calculation

To calculate the 2D PMF of the adsorption of Janus NP on lipid bilayers, we employ a metadynamics method as previously described in the literature.[39-41] Free energy simulation methods play a crucial role in understanding the thermodynamic properties of various biologically important systems and phenomena. These methods are utilized to estimate hydration free energies of ions and small molecules, protein-ligand binding affinities, and protein stability.[42] In the metadynamics simulation, an external history-dependent potential, which is called a bias potential, is added to the selected collective variables (CVs), which alters the system's dynamic behaviour. A collective variable (CV) is a predefined descriptor of the molecular system being studied, and it must be a differentiable function of the atomic coordinates. Furthermore, the value of CV should reflect the state of the simulated system, including metastable states.[43] The FES can be constructed in the space spanned by those CVs. The bias potential $V_{bias}(S, t)$ at time t can be written as:[42]

$$V_{bias}(S,t) = \int_0^t \omega exp\left(-\sum_{i=1}^{d} \frac{(S_i - S_i(t'))^2}{2\sigma_i^2}\right) dt' \qquad (1)$$

where ω is the Gaussian height, which is controlled by the deposition stride, S_i is one of the predefined CVs, and σ_i is the Gaussian width for i^{th} CV. By incorporating a Gaussian distribution-bias potential, this method encourages the system to move away from local minima and towards nearby saddle points on the FES. As a result, the FES becomes more flattened at the end of the simulation. This allows us to estimate the free energy **surface** as a negative imprint of the total bias potential added to the system:[42]

$$F(S) = -V_{bias}(S, t \to \infty) \qquad (2)$$

For the metadynamics run on Janus NPs interacting with lipid bilayer, the centre-of-mass (COM) angle and COM distance are two CVs used to quantify the position and orientation of a Janus NP within a lipid bilayer. The COM angle is defined as the angle between the vector connecting the COM of the Janus NP and the hydrophobic portion of the NP, and the vector connecting the COM of the Janus NP and the centre of the lipid bilayer. The COM distance, on the other hand, is defined as the distance between the COM of the Janus NP and the centre of the lipid bilayer. These CVs are illustrated in **Fig. 3a**. To have a better visualization, **Fig. S3** provides an illustration of the space spanned by the CVs during the metadynamics simulation of

JP50/50 interacting with the pure DOPC membrane. The changes in the CVs over the course of the simulation, as shown in **Fig. S3**, indicate which configurations of the Janus NP-membrane were sampled at a given time when the bias potential was applied according to Equation (**1**). Subsequently, the FES of the interaction was computed using Equation (**2**). The FES provides insights into the thermodynamic behaviour of the nanoparticle-membrane interaction. A lower value of the free energy indicates a more stable and energetically favourable adsorption process. It can aid in understanding the adsorption mechanisms.

The metadynamics simulations are performed using GROMACS v. 2020.6 (modified version) with the addition of Plumed version 2.7.[44] The basic theory about the metadynamics and all the parameter settings can be found on the Plumed web page.[45] The simulations are performed at a temperature of 310 K and Gaussian functions are deposited every 500 simulation steps (equivalent to a time interval of 10 ps) as a common setting in the Plumed. The height of the Gaussian functions is set to be $1.2k_BT$ kJ mol^{-1} and the bias factor, which controls the rate of decrease in the Gaussian height, is set to be 10. The width of the Gaussian functions is defined by the sigma values, which are set to be 0.05 nm for the distance variable and 0.3 (radian) for the angle variable. The range of the COM distance and angle variables are set to 0–30 nm and 0°–180°, respectively.

MD result analysis

The analysis of membrane defects induced by Janus NPs is performed by monitoring the reduction in membrane area.[15] This calculation is depicted in **Fig. S4**. The dimensions of the lipid bilayer are extracted throughout the simulation using the *gmx energy* tool. The number of lipids extracted by Janus NPs is evaluated using the *gmx mindist* tool with a cut-off distance of 0.6 nm from Janus NP beads. The energy of molecular interactions between the Janus NPs and the lipids in the membrane including the LJ and Coulombic interactions, which represent the hydrophobic and electrostatic interactions, respectively, is extracted from MD results using the *gmx energy* tool. Additionally, the diffusivity of lipids in the membrane, which represents the fluidity of the lipid bilayer, is calculated using the *gmx msd* tool. Lipid bilayer's thickness was determined by measuring the distance between the lipid head group (PO4) in the upper and lower layers. The membrane was discretized into small 2 × 2 nm^2 bins. Within each bin, we identified lipid head groups in the upper and lower leaflets and computed the maximum distance between the leaflets. Lipid density was determined using the *gmx densmap* tool with the same 2 × 2 nm^2 binning scheme. Snapshots during the simulation are rendered using the Visual Molecular Dynamics (VMD) software.[46]

Results and Discussion

Effect of Janus balance

As illustrated in **Fig. 1**, our MD simulation results demonstrate that the Janus balance of Janus NPs has a significant impact on their ability to disrupt lipid bilayers. Specifically, as the Janus balance increases, the NPs tend to interrupt lipid bilayers more. The JP 50/50 (50% hydrophobicity) can cause wrinkling of the membrane, similar to what was observed in previous studies.[15, 18] In contrast, the JP 80/20 (20% hydrophobicity) slightly interrupts the membrane, while the JP 90/10 (10% hydrophobicity) fully embeds its hydrophobic portion into the lipid bilayer without causing defects. These computational results are consistent with previous experimental findings, where the Janus balance of 10% hydrophobicity was determined to be the lower threshold that would not generate membrane defects.[14] Our MD simulation results in conjunction with previous experimental findings, confirm that the Janus balance significantly impacts on the ability of Janus NPs to disrupt lipid bilayers.

To further investigate the effect of NP configuration on membrane perturbation, a control model using a uniform amphiphilic NP (JP WM) was also performed and compared to JP 50/50. The bottom snapshot in **Fig. 1b** shows that the JP WM quickly inserts into the membrane within 30 ns, but then remains between the two lipid leaflets with its surface entirely covered by lipids. As a result, the JP WM becomes completely embedded inside the bilayer without inducing membrane wrinkling. This differs from the JP 50/50, where the membrane integrity is compromised. These results confirm the critical role of Janus NP configuration where the anisotropic Janus NPs cause significantly more defects to the GUVs when compared to the uniform amphiphilic NPs.[18] We also perform MD simulations in the case of multiple Janus NPs with different Janus balances interacting with a pure DOPC membrane. Our findings indicate that the results of the multiple Janus NP simulations exhibit a similar trend to those of single Janus NP models. Specifically, we observed that multiple Janus NPs with a Janus balance of 50/50 significantly disrupt the membrane due to the inter-particle effect. This disruptive effect is reduced as the Janus balance decreases (**Fig. S1**). Furthermore, we found that there is no defect and no cooperation between the NPs induced in the membrane for the Janus balance of 90/10. Additionally, we confirmed the impact of an anisotropic configuration when simulating multiple uniform particles. Despite particle cooperative effects, the integrity of the membrane is maintained as two leaflets entirely wrap the uniform particles. These results suggest that the model of a single Janus NP can be employed to represent Janus NP-membrane interactions for the sake of computational efficiency.

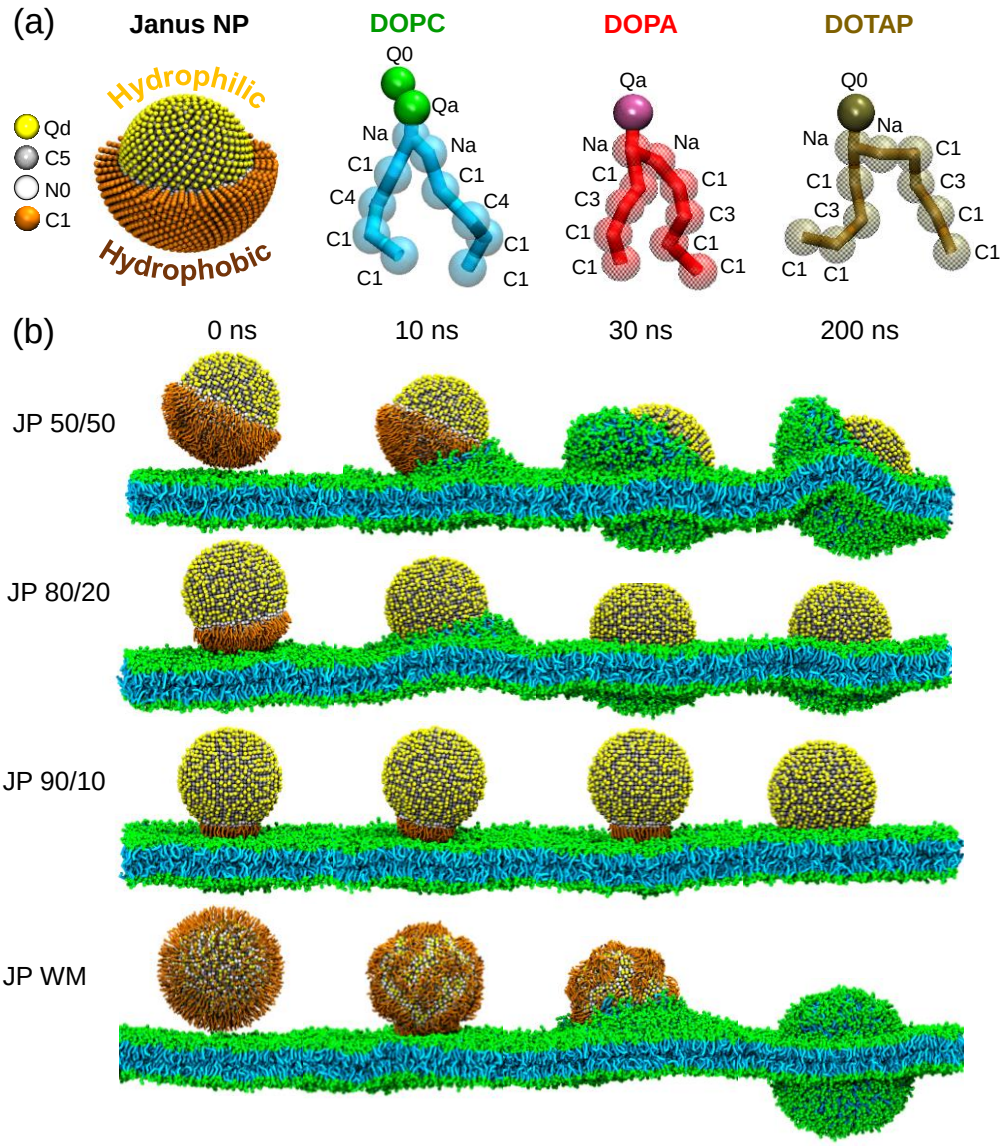

Fig. 1 Janus NP and phospholipid CG models. (a) CG representations of Janus NP and lipids used in the MD simulations. Colouring scheme: Janus NP model includes Au core (grey), sulphur (white), cationic ligand (yellow), and hydrophobic ligand (orange) beads; DOPC molecule contains headgroup (green) and tails (cyan) beads; DOPA molecule contains negatively charged headgroup (purple) and tails (red) beads; DOTAP molecule contains positively charged headgroup and tails beads (brown). The same colouring scheme is used for all MD simulations in this study. (b) Representative snapshots (side view) showing the insertion of Janus NP with different hydrophobicity including JP 50/50, 80/20, 90/10 and well mixed (WM) (core diameter D_{NP} = 10 nm) into a pure DOPC lipid bilayer. The total simulation time for each simulation is 200 ns. The membrane dimension is 23 × 23 × 36 nm^3. In the case of JP WM, the membrane dimension is 35 × 35 × 36 nm^3 to avoid the finite size effect. Solvent molecules are included in the simulation but are not shown here for clarity.

MD simulations were utilized to investigate the main driving forces and mechanisms behind membrane defects induced by Janus NPs during NP-membrane interactions. The advantage of using MD simulations is the ability to access biological events at a molecular scale, which is challenging to experimentalists. By extracting the results from MD simulations for different Janus balances, we aimed to understand how the configuration of the Janus NPs affects the membrane alteration. First, by measuring the area change of the lipid bilayers while encountering the particles, we found that modifying the configuration of the Janus NP can disrupt the membrane differently. The calculation of membrane area change is presented in **Fig. S4**. Our results demonstrate that while JP 50/50 and JP 80/20 significantly influence the membrane alteration, JP 90/10 does not interrupt the lipid bilayer. This is evidenced by the fact that the membrane area remains almost unchanged in the presence of JP 90/10, as shown in **Fig. 2a**. Our findings indicate that the hydrophobic portion of JP 90/10 is completely inserted into the membrane, as seen in the snapshots in **Fig. 1b**. This is likely due to the low coverage of hydrophobic ligands on the particle surface, which constitutes only 10% of the particle surface. Therefore, the insertion of the

JP 90/10's hydrophobic part does not cause any apparent changes in the membrane. In contrast, JP 50/50 significantly reduces the area of the lipid bilayer through the wrinkling effect (**Fig. 1b)**. On the other hand, JP 80/20 expands the area of the membrane up to 10% even though it can slightly bend the membrane. This result implies that even though the JP 80/20's hydrophobic face can completely insert into the lipid bilayer, the Janus balance is not strong enough to extract lipids from the membrane. Hence, this cannot cause the membrane to contract, as observed in the case of JP 50/50. Also shown in **Fig. 2a**, we compared the area reduction induced by uniform amphiphilic nanoparticles (JP WM) to other types of JPs. Our results indicate that, similar to JP50/50, JP WM can effectively reduce the area of the membrane by fully embedding into it and inducing contraction. However, unlike JP50/50, which results in membrane wrinkling, JP WM preserves the structural integrity of the membrane. This is demonstrated by the snapshots in **Fig. 1b** and **Fig. S1**.

Since the area reduction calculation is insufficient to conclude if JP 50/50 is better in terms of membrane reorganization to the random NPs, we calculated other metrics to characterize the NP-membrane interactions. First, we conducted an analysis of the pure DOPC membrane's thickness landscape both before and after interaction with single/multiple JP 50/50 and JP WM nanoparticles (NPs). **Fig. S2b** illustrates that JP 50/50 NPs induced alterations in membrane thickness and generated defects. These defects are represented by white regions in the thickness landscape because of absence of lipid head groups in either the upper or lower lipid layer within specific bins. This defect formation was not observed in the case of JP WM-membrane interaction, despite JP WM's ability to modify membrane structure by changing bilayer thickness. This can be rationalized by examining the top-view snapshots in **Fig. S2a**, where JP WM is embedded within the membrane, preserving membrane integrity. In contrast, JP 50/50 interacted with the membrane at a tilted angle, inducing a significant local imbalance in bilayer thickness and perturbing membrane organization. The introduction of four JP 50/50 NPs is shown to induce much stronger thickness alteration compared to four random NPs and generate more defects compared to individual JP 50/50 NP with defect area percentages of 7.81% and 3.51%, respectively. Furthermore, we calculated the lipid density distribution across the membrane as shown in **Fig. S2c**. We confirm that JP 50/50 NPs exert a more pronounced disruption on local lipid density at interaction sites compared to the uniform NPs, corroborating the thickness findings. Based on this analysis, we assert that JP 50/50 NPs exhibit a more potent disruptive influence on the lipid membrane compared to uniform NPs. This assertion is also supported by experimental data from prior work wherein JP NPs outperformed uniform NPs in generating defects on vesicle membranes at same particle concentrations.[18]

We then utilize several important metrics, including mean square displacement (MSD) of lipids and total energy of LJ interactions between lipids and particles. First, we calculate the MSD of lipids in the membrane during interactions with different Janus NP models to determine the impact of particle insertion on the fluidity (lipid diffusion) of the bilayer. Interestingly, despite variations in disruptive effects, the MSD values of lipids when encountering particles with different hydrophobicity are found to be similar to each other and comparable to those of a non-interrupted lipid bilayer (**Fig. 2b**). This suggests that the effect of a single Janus NP on lipid diffusivity is negligible in this case. Next, we calculate the total LJ interaction energy between lipids and particles for all simulations. The results reveal that the JP 50/50 generates approximately two times higher interaction energy than the JP 80/20 and approximately five times greater than the JP 90/10 (**Fig. 2c**). Our study suggests a linear relationship between the hydrophobicity of Janus NPs and their ability to interact with lipids in the membrane. The dominant LJ interactions induced by the JP 50/50, among other Janus balances, may explain the strong extraction of lipids and severe distortion of the lipid bilayers observed with this NP. This hypothesis is supported by our simulation results, as shown in **Fig. 2d,** which demonstrate that the JP 50/50 can extract double the number of phospholipids compared to the JP 80/20 and approximately four times more than the JP 90/10. Our molecular analysis supports the conclusion that anisotropic Janus NPs with higher hydrophobicity can induce stronger lipid extractions and generate more defects in the lipid bilayers linearly.

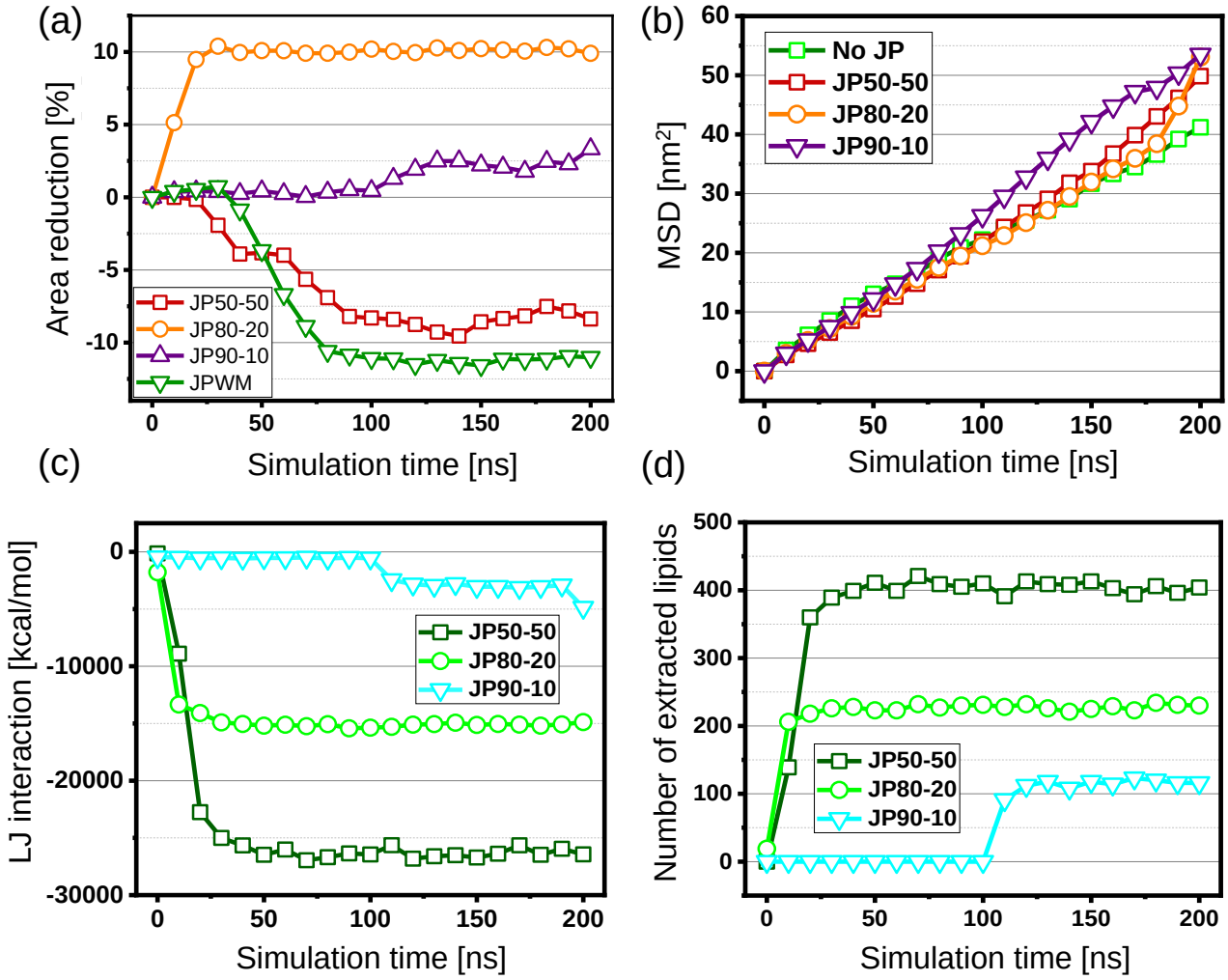

Fig. 2 Effects of Janus balance on (a) membrane area reduction, (b) lipid fluidity (means square displacement), (c) LJ interaction energy between Janus NP and lipid membrane, (d) number of extracted lipids induced by Janus NP.

After that, we investigate the mechanism of NP–membrane interactions in terms of thermodynamics. Specifically, we focus on the impact of Janus balance on the FES of Janus NP-membrane interactions. Given the anisotropic nature of Janus NP, it is necessary to consider two CVs, as opposed to the traditional umbrella sampling approach of considering only the distance between two atoms or groups. Specifically, we focus on the distance and angle between the COM points of the Janus NP and the lipid bilayer (**Fig. 3a**). The COM distance provides insight into the thermodynamic favourability of the insertion of the Janus NP into the membrane. The COM angle specifies the preferred tilted angle of the Janus NP relative to the membrane upon encounter. Subsequently, the 2D metadynamics simulations are performed on various Janus balances using Plumed version 2.7.[44] As depicted **in Fig. 3,** increasing hydrophobic coverage leads to more thermodynamically favourable interactions between the particle and the lipid bilayer.

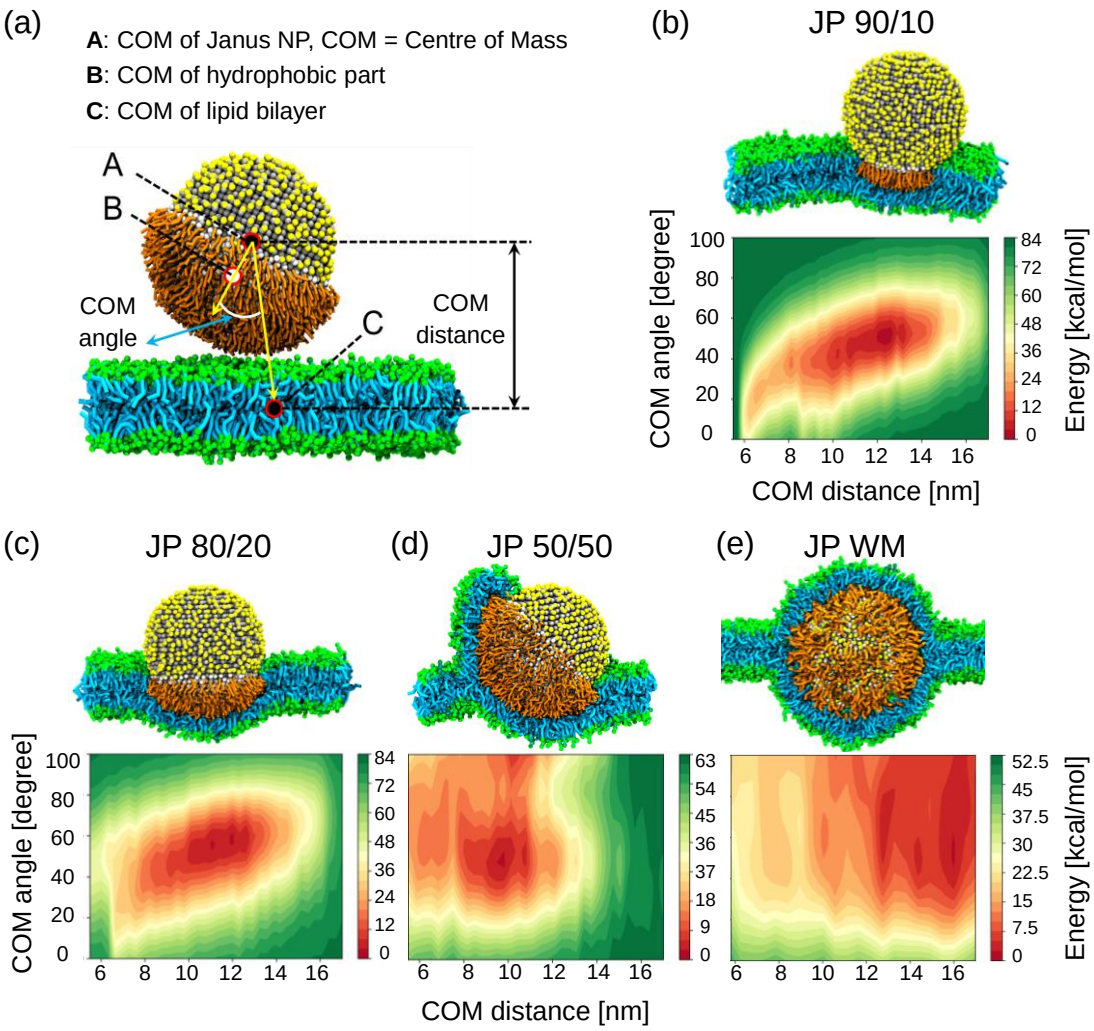

Fig. 3 FES of interaction between Janus NPs with different Janus balances and pure DOPC lipid bilayers. (a) Two reaction variables used for 2D PMF calculations include COM distance and COM angle (COM is centre-of-mass). The COM angle is defined as the angle between the vector connecting the COM of the Janus NP and the hydrophobic portion of the NP, and the vector connecting the COM of the Janus NP and the centre of the lipid bilayer. The COM distance is defined as the distance between the COM of the Janus NP and the centre of the lipid bilayer. Cross-sectional snapshots and FES of interaction between pure DOPC membrane with (b) JP 90/10, (c) JP 80/20, (d) JP 50/50 and (e) JP WM. Janus NP core's diameter is 10 nm. The membrane dimension in (a), (b), (c), (d) is 23 × 23 × 36 nm^3. The membrane dimension in (e) is 35 × 35 × 36 nm^3 to avoid the finite size effect. Solvent molecules are included in the simulation but are not shown here for clarity.

This is evident in the FES plots, where a reddish colour represents the lower energy regions, while green indicates high energy-barrier areas for the NP-membrane interaction. Our analysis reveals that the energetically favourable region in the FES plot of JP 90/10 is relatively narrow (**Fig. 3b**). Additionally, the high energy-barrier area is larger than other Janus balances. As the hydrophobicity of the Janus NP increases, the low free energy area, represented by the reddish colour, is observed to expand, indicating that the NP is more favourable for interaction with the membrane. Furthermore, the favourable binding area in the case of 50% hydrophobicity is significantly large in both the COM distance and angle coordinates compared to the case of lower hydrophobic coverages. We found that while it is challenging to insert JP 90/10 and JP 80/20 deeper into the membrane (**Fig. 3b** and **3c**), the JP 50/50 can penetrate the membrane and surpass a COM distance of 6 nm (**Fig. 3d**). Additionally, we observed that Janus NPs with different Janus balances tend to adopt a preferred angle of approximately 40°–60° relative to the planar membrane, as reported in our previous studies.[15, 18] Importantly, this is the first 2D PMF calculation to demonstrate that the tilted configuration of the Janus NP is the most favourable state when encountering lipid bilayers. This is also associated with the wrinkling effects that Janus NPs can induce on lipid membranes.[18] To further verify the metadynamics simulation, we conducted additional tests on JP WM and observed some

intriguing behaviour. Due to the uniformity of JP WM, we randomly selected a point on its surface instead of the COM of the ligand part to represent the angle used in the metadynamics. As seen in **Fig. 3e**, the angle range that favours JP WM-membrane interaction is significantly broader and more global compared to other JPs. This result can be attributed to the isotropic configuration of JP WM, which ensures that hydrophobic interaction is uniformly distributed across the membrane. Thus, there is no preferred angle for interaction between the uniform particle and the membrane. In conclusion, our 2D thermodynamic calculations confirm that: 1) Janus NPs interact with lipid bilayers with a preference for a tilted angle, and 2) Janus NP with a Janus balance of 50/50 possess a favourable FES when encountering lipid bilayers, leading to a more significant perturbation effect on the membrane as shown in **Figs. 1** and **2**.

Effect of negatively charged lipid concentration

In biological membranes, various phospholipid types with different charge states are present, providing functions such as the uptake of specific proteins.[16, 47-49] For example, bacterial cell membranes contain a significant amount of anionic lipids, which enhances the selectivity of cationic antibacterial agents.[50] Therefore, it is essential to study the interaction of Janus NPs with different charged phospholipid bilayer systems for further biomedical applications. In this study, we focus on the influence of anionic lipids in the membrane by using a fixed Janus balance (JP 50/50) for all simulations. The molar concentration of the anionic phospholipid, DOPA, in DOPC lipid bilayers varies from 0 to 20%. MD simulations were performed on different anionic lipid bilayers, and the snapshots of NP-membrane interactions were collected for 200 ns (**Fig. 4a)**. The results of our simulation indicate that increasing the negative charge of lipids in the membrane leads to greater disruption of the membrane surface by Janus NPs. Through the analysis of projected area reduction over the duration of the simulation, we observed a monotonic relationship between the concentration of DOPA and the alteration of the membrane (**Fig. 4b**). Specifically, a higher number of negative lipids in the bilayer leads to a more pronounced compression of the membrane induced by the Janus NPs. When we compared the trend of JP50/50 with JP WM, we found that the area reduction induced by JP WM does not significantly change as the anion lipid concentration increases. This suggests that the uniform NP does not strongly prefer the anion lipid membrane. On the other hand, the anisotropic JP is more effective in disrupting membranes with higher negative charges. This is clearly demonstrated in **Fig. 4b**, where JP 50/50 causes double the area contraction induced by JP WM at a DOPA concentration of 20%. As depicted in **Fig. S5**, increasing DOPA concentration enhances electrostatic interactions between JP 50/50 and lipids. This effect is less prominent for JP WM, which contributes to JP 50/50's superior disruptive potential on anionic membranes in comparison to JP WM. We suggest that the extended alkyl chain covering the entire surface of JP WM can obstruct the interaction between its positively charged single beads and anionic lipids in the membrane. In contrast, JP 50/50's distinct hydrophobic and hydrophilic segments can facilitate unimpeded electrostatic attraction to lipid bilayers. This anisotropic configuration of JP 50/50 enhances interactions with the membrane in terms of hydrophobic and electrostatic aspects. This result strongly supports the ability of anisotropic NPs to disrupt anionic membranes, compared to uniform NPs.

Additionally, we evaluated the membrane fluidity by determining the MSD of the lipids in the membrane. We found that the presence of DOPA can nonlinearly reduce lipid diffusivity when interacting with the Janus NP (**Fig. 4c**). To further understand the underlying mechanisms of the observed distorting behaviour, we also calculated the LJ and Coulomb interactions between the Janus NP and the phospholipids in the membrane throughout the simulation. Interestingly, we found that the LJ interactions are consistent across different concentrations of anionic lipids, as observed in **Fig. 4d**. However, the electrostatic interactions between the NP and the membrane become more linear as the concentration of DOPA increases (**Fig. 4e**). This result is noteworthy, given that the Janus NP has a positive hemisphere coverage (Qd beads) on its core surface, which favours interactions between the Janus NP and anionic lipid heads in the membrane. Increased molecular interactions between the Janus NP and membranes containing higher DOPA concentrations result in a higher number of phospholipids extracted from the lipid bilayer, leading to more defects, as previously reported in experimental results.[17] It is worth noting that we only placed the hydrophobic portion of the particles towards the membrane to ensure a consistent initial state for all MD simulations. Furthermore, when the positive hemisphere of the Janus NP faces the membrane, it significantly alters the membrane structure (**Fig. S6a)**. These results, presented in **Fig. 4** and **S6a**, demonstrate the favourable interaction between the Janus NP and negatively charged membranes, which is linearly proportional to the anionic lipid concentration.

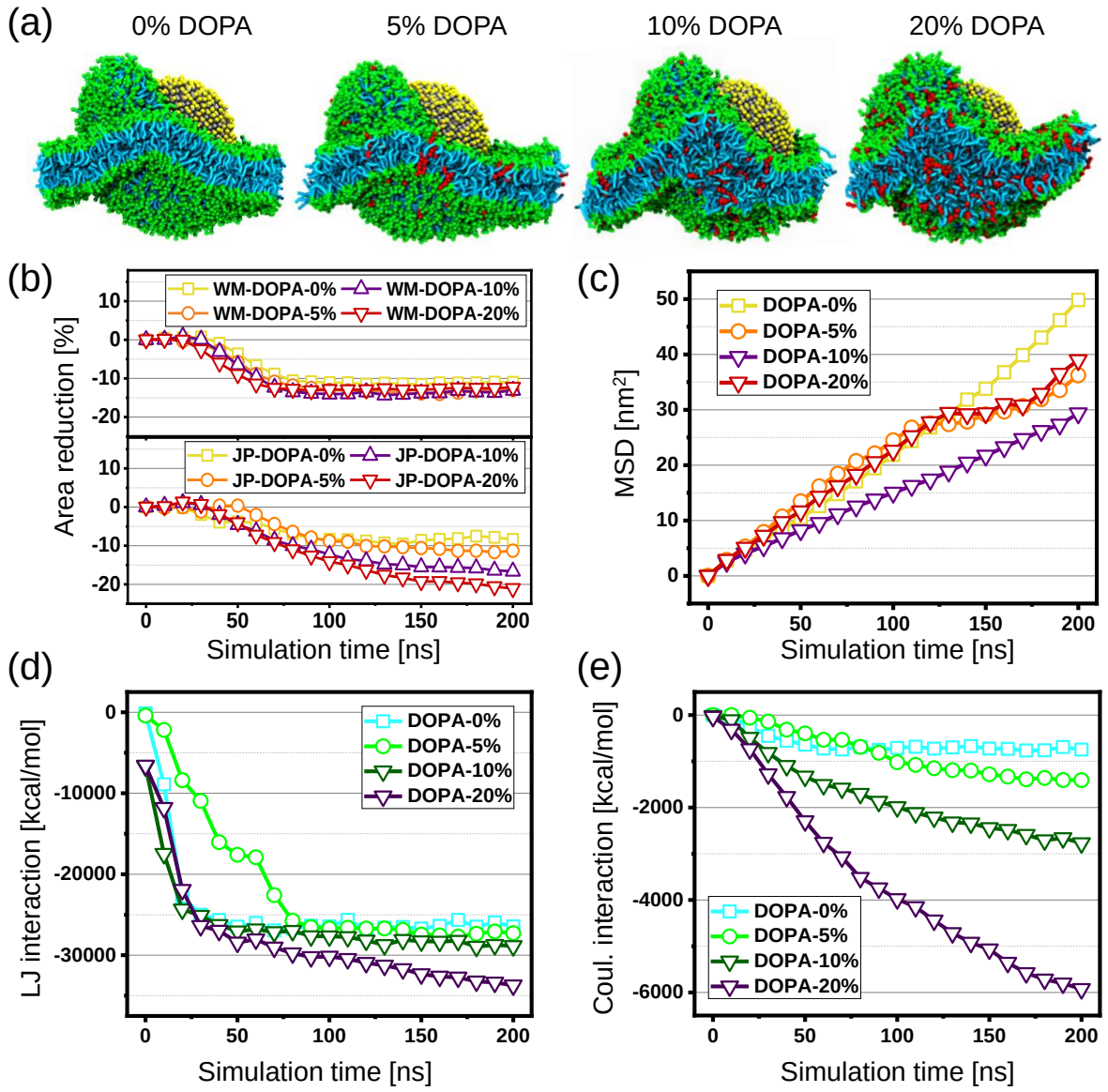

Fig. 4 Effects of anionic lipid concentrations on membrane alteration as depicted by (a) snapshots of MD simulations with different DOPA concentrations at 200 ns, (b) membrane area reduction, (c) membrane fluidity, (d) LJ interaction, and (e) Coulomb interaction. Janus NP core's diameter is 10 nm. The membrane dimension is 23 × 23 × 36 nm^3. Solvent molecules are included in the simulation but are not shown here for clarity.

Effect of positively charged lipid concentration

In addition to anionic phospholipids, cationic lipids also play a crucial role in the function and structure of biological membranes. One example of this is the creation of a transmembrane potential or electrophysiology.[16] In this section, we aim to investigate the effect of cationic phospholipids on the interactions between Janus NPs and membranes. To do this, we varied the molar concentration of DOTAP, a positively charged phospholipid, in a DOPC membrane (**Fig. 5a**). Our results showed that the membrane area reduction induced by the particle in DOPC/DOTAP mixed lipid bilayers is not monotonically affected by the amount of DOTAP. Interestingly, we observed that concentration of 5% or 10% DOTAP significantly reduces the membrane area (**Fig. 5b**). However, when the concentration of DOTAP increased to 20%, the membrane behaviour became similar to that of a pure DOPC bilayer. We then compare the area reduction induced by JP 50/50 to that of the JP WM used as a control sample. Our analysis reveals a similar trend between JP 50/50 and the JP WM. We observe that the JP WM can contract the membrane, but the contraction effect is not proportional to the DOTAP concentration. Specifically, at the concentration of 20% DOTAP, the JP WM shows the worst area reduction among other DOTAP concentrations, which is consistent with the findings for JP 50-50. Therefore, we conclude that the presence of cationic lipids

in the membrane does not significantly impact the interaction between anisotropic/uniform NPs and membranes.

Furthermore, the membrane fluidity of cationic phospholipids decreases as the number of cationic phospholipids increases, similar to the effect observed with the presence of DOPA (**Fig. 5c**). Also, the presence of DOTAP does not significantly influence the LJ interactions between the particles and the lipids in the membrane (**Fig. 5d**). However, unlike the effect of DOPA, the electrostatic interaction energy between the Janus NPs and phospholipids does not monotonically increase as the amount of DOTAP increases (**Fig. 5e**). The intensity of electrostatic interactions is insignificant in comparison to that of LJ interactions (less than 40-fold). Therefore, it is suggested that electrostatic interactions do not significantly contribute to the ability of the Janus NPs to interact with a positively charged membrane. This is further supported by the results of a MD simulation, as depicted in **Fig. S6b**, which shows that when the positive portion of the Janus NP is placed toward a 20% cationic lipid membrane, no interactions occur between them after 100 ns. These findings align with previous experimental work,[17] which also observed that the effect of DOTAP on membrane defects is not significant when compared to the effect of DOPA.

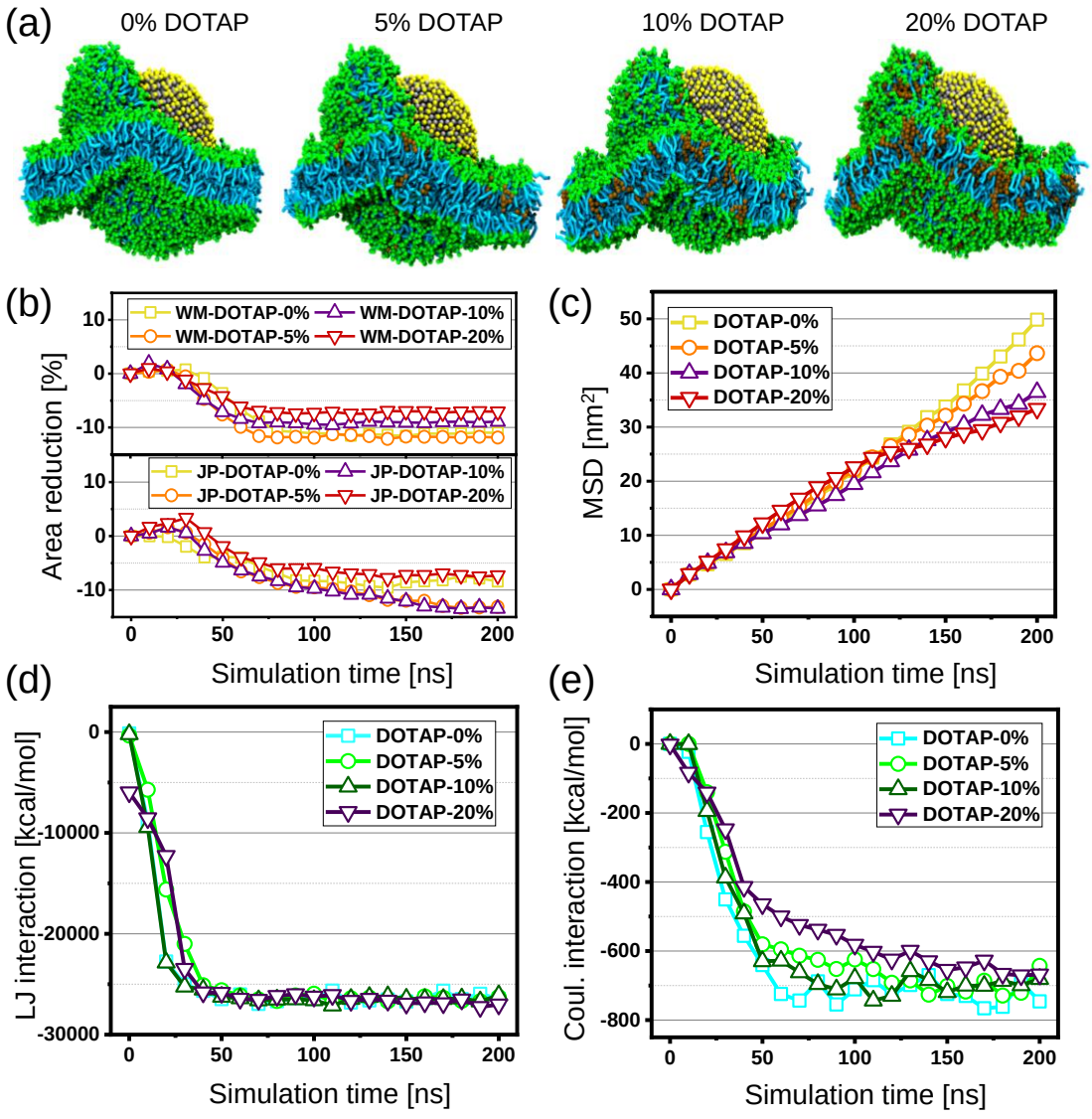

Fig. 5 Effects of positively charged lipid concentrations on the Janus NP-membrane interactions as depicted by (a) MD simulation snapshots at 200 ns, (b) membrane area reduction, (c) lipid fluidity, (d) LJ interaction, and (e) Coulomb interaction. Janus NP core's diameter is 10 nm. The membrane dimension is 23 × 23 × 36 nm^3. Solvent molecules are included in simulation but are not shown here for clarity.

We next examine the FES of the interaction between the Janus NP (JP 50/50) and various surface-charged membranes

(anionic or cationic) using the 2D PMF calculation. Two extreme cases were investigated, including membranes containing 20% DOPA and 20% DOTAP in DOPC to compare with the case of pure DOPC membrane. The results, as illustrated in **Fig. 6**, indicate that the presence of a high concentration of DOPA significantly enhances the interaction between the Janus NP and the membrane. Specifically, in the case of DOPA 20%, we observed a larger low-energy area of interaction between the nanoparticle and the membrane, as indicated by the reddish region in Fig. 6b. Furthermore, although the most stable state is quite similar among the compositions, the range of angles at which the Janus NP can bind to the DOPA 20% membrane is broader. This suggests the presence of more transition states and more opportunities for the Janus NP to interact with the membrane. Importantly, not only the hydrophobic part of the Janus NP, but also the positive hemisphere of the particle can target the membrane, leading to greater membrane distortion, as illustrated in the snapshot in **Fig. 6b** and **Fig. S6a**. Taken together, these findings indicate that the 20% DOPA composition is more favourable for the nanoparticle-membrane interaction, owing to the larger low-energy area of interaction and greater flexibility in binding angles.

Furthermore, when the Janus NP inserts into the 20% DOPA membrane, the NP-membrane interaction is still likely to occur, as evidenced by a larger range of favourable interacting angles when the Janus NP-membrane distance decreases (**Fig. 6b**). In contrast, the FES becomes narrower as the distance decreases for the neutral (**Fig. 6a**) and positively charged (**Fig. 6c**) membranes. Also, we found that the adding cationic phospholipids has minimal effect on the free energy of interaction between the Janus NP and the membrane. When comparing the FES results between different membrane systems, it becomes apparent that the Janus NPs have a more substantial disruptive effect on negatively charged membranes in terms of thermodynamics. These findings suggest that Janus NPs have the potential to selectively target negatively charged bacterial membranes, making them a promising candidate for use as an antimicrobial NP.

Combination effects

In this section, we investigated the combined effects of Janus balance and charged lipid concentration on membrane disruption in Table 2. Four Janus balances are examined, including JP 90/10, JP 80/20, JP 50/50, and JP WM, respectively. We utilize a total of nine different membrane systems, which are composed of various charged lipid concentrations, including 5%, 10%, and 20% DOPA in DOPC: 5%, 10%, and 20% DOTAP in DOPC, pure DOPC, pure DOPA, and pure DOTAP. All MD simulations were conducted for a minimum of 200 ns to reach a stable state for the interaction between a single Janus NP and a membrane, as demonstrated in **Fig. 1b** and previous research.[15]

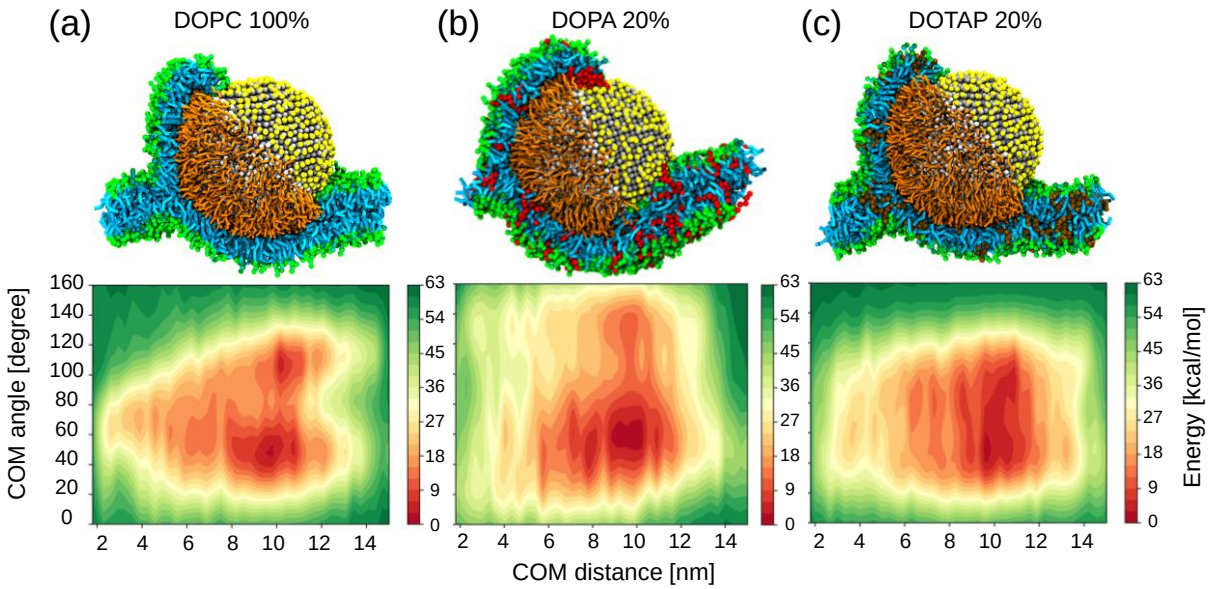

Fig. 6 Effect of negative and positive phospholipid contents on the free energy surface of the interactions between JP 50/50 and different membrane systems. (a) DOPC 100%, (b) 20% DOPA/DOPC and (c) 20% DOTAP/DOPC membranes. The COM angle is defined as the angle between the vector connecting the COM of the Janus NP and the hydrophobic portion of the NP, and the vector connecting the COM of the Janus NP and the centre of the lipid bilayer. The COM distance is defined as the distance between the COM of the Janus NP and the centre of the lipid bilayer. These parameters are illustrated in **Fig. 3a**. DOPA is represented by the red beads, while DOTAP is represented by the brown beads. Janus NP core's diameter is 10 nm. The membrane dimension is $23 \times 23 \times 36$ nm^3. Solvent molecules are included in the simulation but are not shown here for clarity.

As presented in **Table 2**, our findings suggest that a JP 80/20 ratio represents the minimum threshold for Janus balance required to induce distortions and defects in lipid membranes. Additionally, when the anionic phospholipid concentration in the membrane exceeds 10%, Janus NP with a 10% hydrophobicity is also capable of causing defects in negatively charged bilayers. Notably, when the membrane is composed solely of negatively charged lipids, any Janus NPs, regardless of their hydrophobicity or configuration, will ultimately disrupt the membrane's integrity. In contrast, uniform NPs (JP WM), with the exception of 100% DOPA membrane, do not affect the integrity of lipid bilayers and are thus less effective at causing defects compared to anisotropic Janus NPs. These results indicate that Janus NPs are superior to conventional uniform particles in terms of their ability to disrupt phospholipid membranes.

** Combination effects of the Janus balance and ionic lipid concentration on membrane defects and diffusivity:* We found that increasing DOPA concentration leads to a monotonic increase in membrane defects, regardless of the Janus balance (**Fig. 7a**). This suggests that the negatively charged lipids have a strong impact on membrane disruptions. However, the effect of positively charged lipids (DOTAP) on membrane defects remains inconclusive. At 5% or 10% DOTAP, the lipid bilayer was observed to be more compressed, but as the DOTAP concentration increased, the behaviour of the membrane became similar to that of a neutral membrane. Additionally, our findings indicate that the Janus balance has a significant impact on membrane deformation. The JP 50/50 is found to alter all membranes, regardless of the lipid composition. In contrast, the JP 90/10 has a negligible impact on membrane deformation. The JP 80/20, on the other hand, has a tendency to insert its hydrophobic portion into the membrane, resulting in an enlargement of the membrane area. In terms of the combined effect on membrane fluidity, the lipid diffusion-reducing effect of DOPA concentration is pronounced, while the effect remains uncertain with DOTAP (**Fig. 7b**). Specifically, the presence of anionic phospholipids reduces the diffusivity of lipids, regardless of the configuration of the Janus NP. However, the lipid diffusivity in cationic membranes is not as significantly reduced by the DOTAP amount, with the exception of JP 50/50. The impact of Janus balance on membrane fluidity is uncertain. Specifically, increasing the Janus balance can reduce lipid diffusion in the case of 10%, 20% DOPA, and 20% DOTAP bilayers. On the other hand, Janus balance modification can arbitrarily accelerate or reduce lipid diffusivity in other lipid membranes (**Fig. 7b)**. Based on these observations, it can be concluded that Janus balance does not have a significant impact on lipid diffusivity in this study.

Table 2 Combination effect investigated in this work. Janus NP core's diameter is 10 nm. The membrane dimension is 23 × 23 × 36 nm^3 when using anisotropic Janus NP models (JP 50/50, JP 80/20 and JP 90/10) or 35 × 35 × 36 nm^3 when using uniform particle models (JP WM) to mitigate the finite effects of planar membranes.

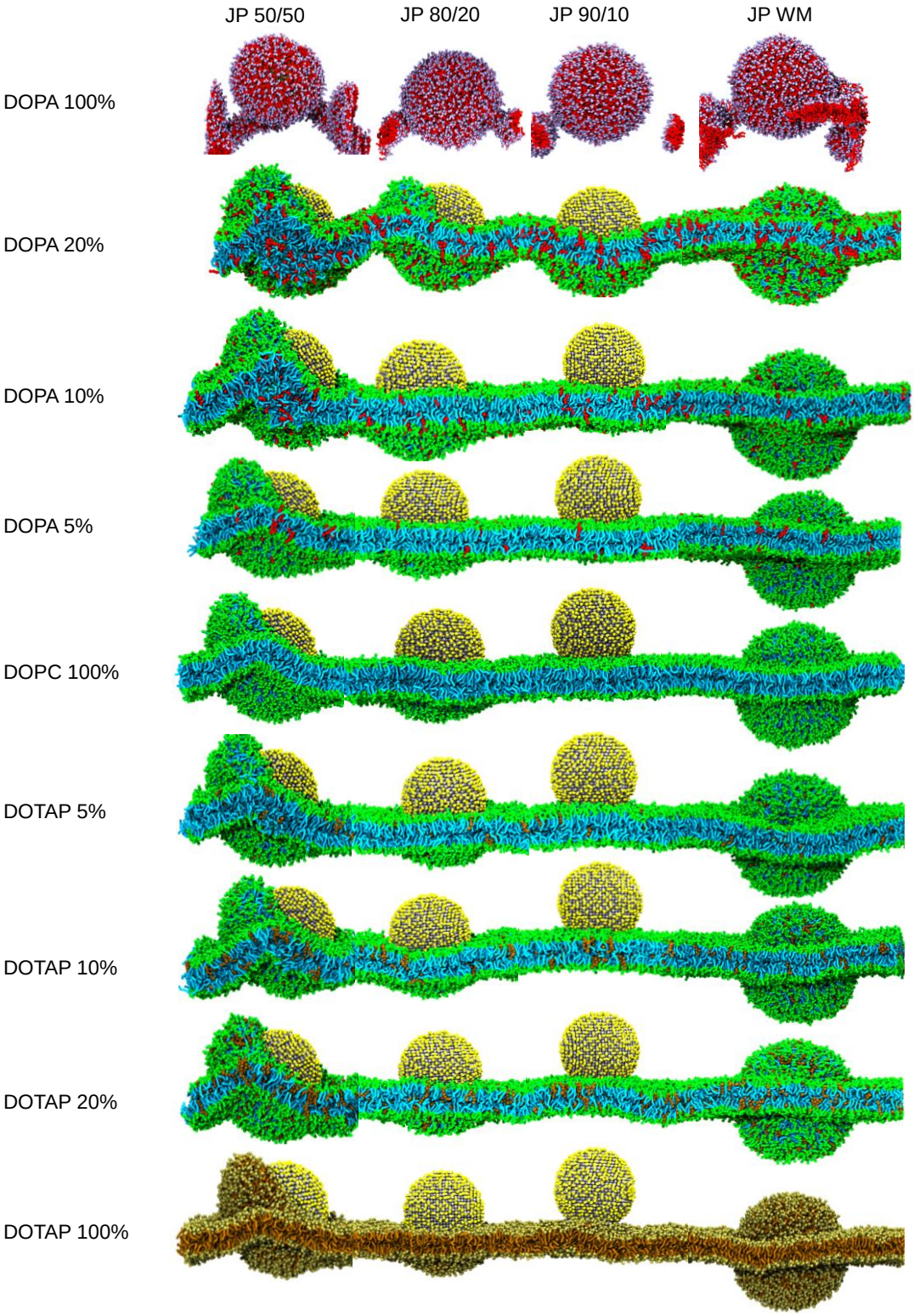

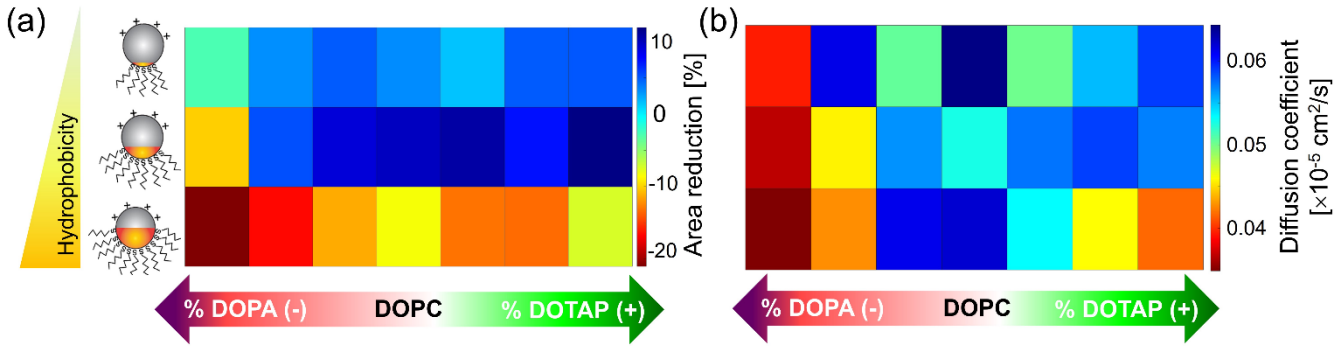

Fig. 7 Combination effect of Janus balance and charged lipid concentrations on (a) membrane area reduction, and (b) membrane fluidity. The illustration of Janus NPs is adapted from Yu et al.[14] The molar concentrations of DOPA and DOTAP vary in ascending order from 5% to 20%. Pure DOPC membrane (neutral membrane) is referred to as DOPC. The Janus balance varies and includes JP 50/50, JP 80/20, and JP 90/10 (from bottom to top). The results are obtained from an averaging of three independent MD simulations.

* *Combination effects on NP-membrane molecular interactions:* The study of the interaction energy between Janus NPs and phospholipids in the membrane at the molecular scale can provide insight into the mechanisms underlying different NP-membrane interfacial behaviours. As shown in **Fig. 8a**, increasing the concentration of negatively charged lipids in the membrane leads to stronger LJ interactions between the NP and the lipids. However, the influence of DOTAP content on the LJ interactions is negligible. Additionally, the degree of Janus hydrophobicity has a significant impact on the LJ interaction. Higher coverage of hydrophobic ligands enhances the NP-membrane interaction and lipid extraction, regardless of the charge of the membrane, leading to increased extraction of lipids and defects in the bilayer. Additionally, we observed that electrostatic interactions also play a significant role in generating defects in negatively charged lipid bilayers, as the amount of DOPA in the bilayers increases (**Fig. 8b**). However, this effect is less pronounced when varying the concentration of DOTAP. When analysing the interactions between the NPs and negatively charged lipid bilayers, it was found that both hydrophobic and electrostatic interactions contribute to the formation of defects in the bilayer. Conversely, in positively charged membranes, the hydrophobic interaction is dominant, and the electrostatic interaction plays a minimal role in forming defects. In conclusion, these results highlight the importance of hydrophobic interactions in the disruption of lipid membranes by Janus NPs and the efficient disruptive effect of these NPs on negatively charged membranes.

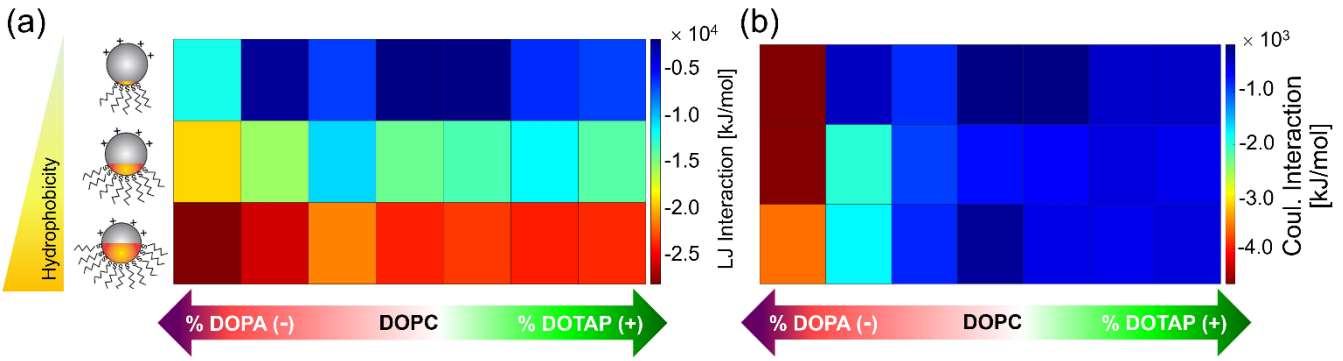

Fig. 8 Combination effect of Janus balance and charged lipid concentrations on (a) LJ and (b) Coulomb interactions. The illustration of Janus NPs is adapted from Yu et al. [14] The molar concentrations of DOPA and DOTAP vary in ascending order from 5% to 20%. Pure DOPC membrane (neutral membrane) is referred to as DOPC. The Janus balance varies and includes JP 50/50, JP 80/20, and JP 90/10 (from bottom to top). The results are obtained from an averaging of three independent MD simulations.

Implement on bacterial membrane-mimicking model

In order to investigate the applicability of our computational model in a biologically realistic context, we conduct MD simulations of Janus NPs with a 50/50 Janus balance interacting with a bacterial-mimicking lipid membrane. The Janus balance of 50/50 was chosen as it has been previously shown to exhibit the strongest disruptive activity among the other Janus balances investigated. The lipid membrane model is composed of LPS and POPC lipids, mimicking the gram-negative bacterial membrane.[51] The CG beads of LPS and POPC are presented in **Fig. S7** and **Table S1**. We evaluate the impact of different molar concentrations of LPS in a POPC membrane, specifically 5% and 20%, on the NP-membrane interaction. Our results show that increasing the concentration of LPS in the POPC membrane does not enhance the NP-membrane interaction but reduces the ability of the Janus NP to disrupt the membrane.

Specifically, at a concentration of 5% LPS in the membrane, the Janus NP with a COM angle of 0°, where the hydrophobic portion faces directly toward the bilayer, can effectively interact with the POPC lipids in the membrane. This results in wrinkling of the membrane due to hydrophobic interactions after 500 ns (**Fig. 9a**). However, when the LPS content is increased to 20%, the Janus NP struggles to immerse into the LPS/POPC membrane when placed above the membrane with the same COM angle of 0° (**Fig. 9b**). These findings suggest that the outer and inner core LPS may inhibit hydrophobic interactions between the Janus NP and lipids, thereby preventing lipid extraction caused by the Janus NP. This implies that LPS molecules may have a similar role in stiffening the membrane as cholesterol in lipid bilayers.[52-54] This is confirmed with the higher order parameters of the lipid tails in the LPS/POPC membrane when compared to the lipids in the DOPC/DOPA membranes (**Fig. S8**). To further investigate this, we then reverse the initial orientation of the Janus NP so that the positive portion of the Janus NP faces toward the LPS/POPC membrane (COM angle of 180°). This change was implemented to facilitate electrostatic interactions between the Janus NP and the negatively charged lipids (LPS) present in the membrane, as observed in **Fig. S6a** for a DOPC/DOPA membrane. However, the simulation results show that the Janus NP only adheres firmly to the surface of the membrane via electrostatic attraction between the positive beads on the surface of the Janus NP and the LPS and does not cause any defects as well (**Fig. 9b**).

Eventually, we examined the scenario in which both parts of the Janus NP simultaneously contacted the membrane depicted in **Fig. 9b** (COM angle of 90°). Notably, we found that this configuration enhances the combination of hydrophobic and electrostatic interactions between the Janus NP and the LPS/POPC membrane, leading to bilayer wrinkling after 500 ns. To further assess the effectiveness of JP 50/50 in disrupting the bacterial membrane, we conducted a comparison with JP WM in **Fig. 10**. We ran two simulations of these nanoparticles and measured the reduction in area induced by them. Our findings indicate that while JP 50/50 can successfully disrupt the membrane, extract the lipids, and contract the LPS membrane, the uniform NP simply remains suspended above the membrane without extracting any lipids or causing any membrane disruption. Consequently, while anisotropic NPs are able to reduce the membrane area by roughly 5% after 1000 ns, uniform NPs fails to contract the membrane and allow the membrane to survive. In response to the limited reduction in the area of the LPS/POPC membrane by a single JP 50/50, we tested the potential of multiple Janus NPs to represent elevated JP concentrations encountered in real-world scenarios (**Fig. S9**). The outcomes revealed that increasing JP concentration leads to a notable threefold reduction in membrane area. This effect arises from the collaborative influence exerted by multiple JPs, as also shown in our prior research.[55] Based on this analysis, it is affirmed that JP 50/50 effectively exhibits disruptive properties towards the LPS/POPC membrane.

The findings of our study confirm two important points. Firstly, they demonstrate the significance of the anisotropic configuration of Janus nanoparticles in membrane disruption. Secondly, they suggest that the current design of Janus nanoparticles has potential antibiotic activity. Previous studies have highlighted the ability of nanoparticles to disrupt bacterial cell membranes, which is one of their antibiotic activities as reported in the literature review.[56-58] For instance, Yusong Tu et al. explored the possibility of using graphene nanosheets as an antibacterial treatment by demonstrating their ability to disrupt bacterial membranes through area cutoff (type A) and lipid extraction (type B) mechanisms, via computational simulations and experiments.[59] By calculating the number of extracted lipid over the course of simulations (**Fig. S10**), we found that a single JP 50/50 has the capacity to extract a substantial proportion of lipids from the membrane, specifically up to 30.9% (362 lipids out of a total of 1170 lipids). Notably, this lipid extraction remains noteworthy even in cases where the reduction in area is not substantial. This observation claims the potential antibiotic properties of single Janus NP as type B mechanism. Further, at higher concentrations, JP 50/50 NPs exhibit antibiotic potential against both type A and type B due to their dual capability of significantly reducing membrane area by 18% and extracting up to 31.5% of lipids (equivalent to 716 lipids out of a total of 2270 lipids) within the membrane. Based on this evidence, it seems reasonable to consider our Janus NP design as a potential candidate for antibiotic applications. While additional experimental validation is necessary to confirm their efficacy, Janus NPs hold promise as a valuable addition to the arsenal of antibiotics in the ongoing battle against bacterial infections.

In light of these results, further investigations can be developed to optimize the configuration of Janus NPs for potential antibiotic applications. One promising avenue for modification includes the incorporation of more effective ligands, such as antimicrobial peptides amphotericin,[60] polymyxin,[60, 61] cyclodextrin derivatives,[62] crown ether urea derivatives,[63] small molecules that contain boronic acid and

urea functionalities,[64] and small aromatic molecule JD1, [65] which have been previously shown to target bacterial membranes selectively.

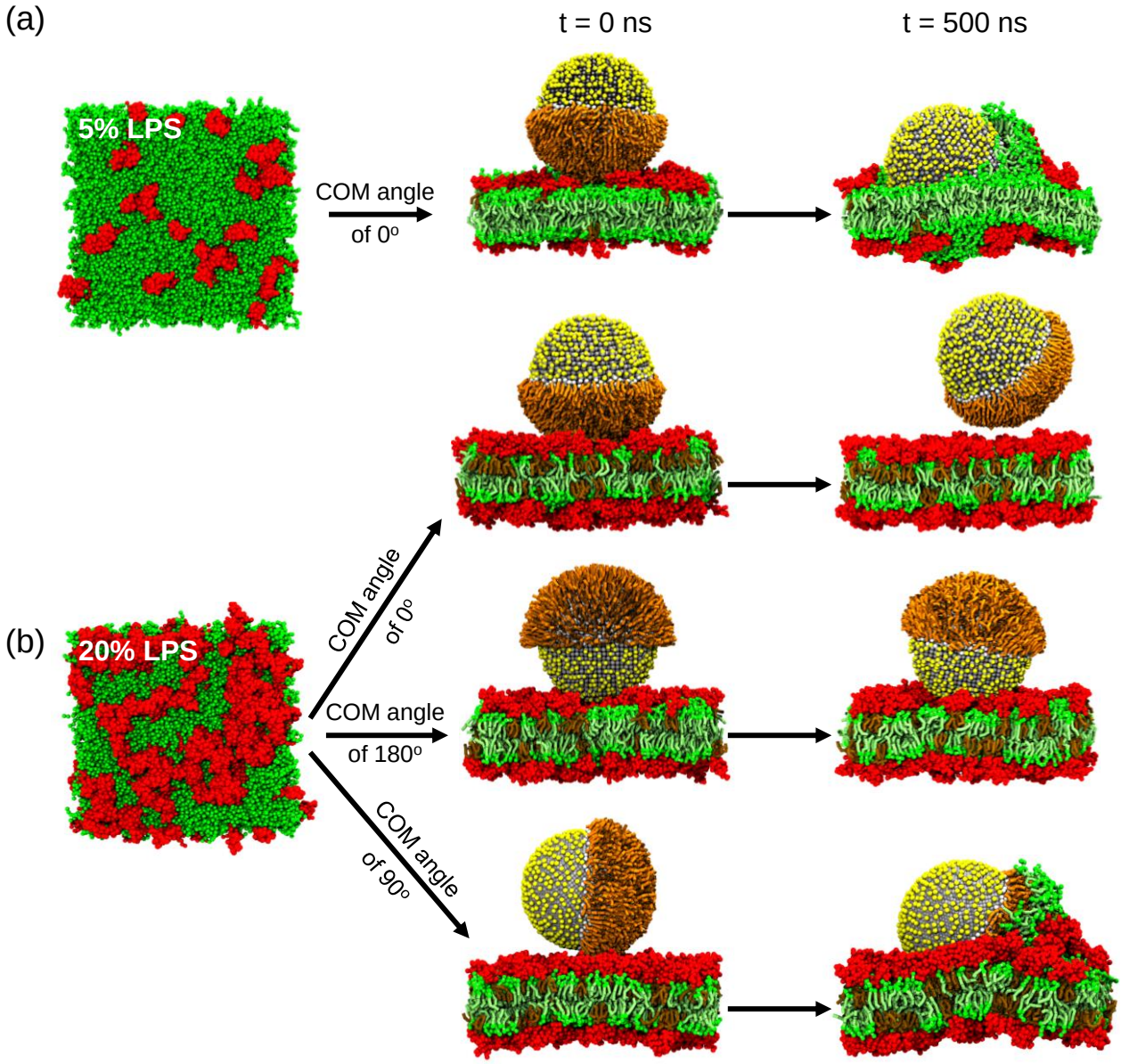

Fig. 9 Models of bacterial membrane (LPS/POPC) with 5% of LPS and 20% of LPS (bacterial membrane-mimicking models) after MD simulations for 500 ns. MD snapshots of interactions between JP 50/50 and (a) 5% LPS/POPC membrane with the COM angle of 0°; (b) 20% LPS/POPC membrane with three different initial states of Janus NP (COM angles of 0°, 180° and 90°). The COM angle is defined as the angle between the vector connecting the COM of the Janus NP and the hydrophobic portion of the NP, and the vector connecting the COM of the Janus NP and the centre of the lipid bilayer. This parameter is illustrated in **Fig. 3a**. POPC molecule contains headgroup beads (green) and tails (lime). LPS molecule contains outer and inner core saccharides (red) and lipid A (brown). Janus NP core's diameter is 10 nm. The membrane dimension is 23 × 23 × 36 nm^3. Solvent molecules are included in the simulation but are not shown here for clarity.

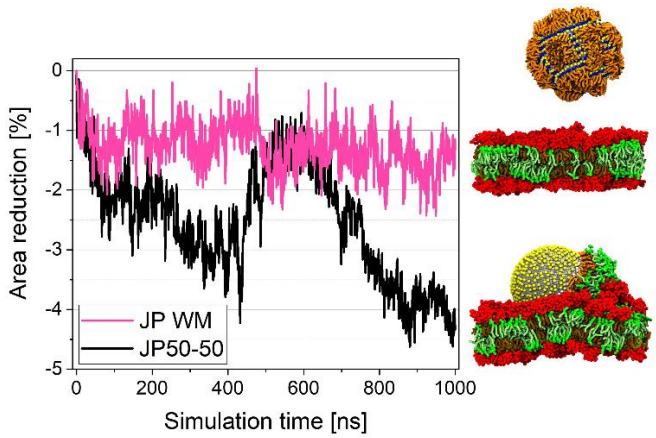

Fig. 10 Comparison of the disruption between JP 50/50 and JP WM toward the 20%LPS/POPC membrane. Snapshots of JP WM (top) and JP 50/50 (bottom) taken at 500 ns show that JP 50/50 can disrupt and extract the lipids out of the membrane, whereas JP WM shows no such effect. Janus NP core's diameter is 10 nm. The membrane dimension is 23 × 23 × 36 nm^3. Solvent molecules are included in the simulation but are not shown here for clarity.

Conclusions

In this study, we systematically investigated the disruption of lipid bilayers induced by amphiphilic Janus NPs using CGMD MARTINI simulations. Our results demonstrate the combined effects of Janus balance (hydrophobicity) and charged lipid contents on the interactions between Janus NPs and membranes. The behaviour of Janus NPs with different Janus balance was found to cause varying levels of membrane disruption. More importantly, JP 50/50 displayed a wrinkling effect that differed from the conventional uniform NP. While this wrinkling effect had been previously observed experimentally, here we utilized MD simulations to explain the underlying mechanism at the molecular level. Our simulation results help to demonstrate why Janus NPs generate more defects in lipid membranes than uniform NPs, as observed in experiments. This work highlighted the potential of utilizing Janus NPs to disrupt biological membranes in a superior manner compared to conventional NP design. In addition, our research demonstrated that Janus NPs have a significant impact on disrupting negative membranes compared to uniform NPs with similar hydrophobic and hydrophilic coverage. We also provided valuable insights into the molecular mechanisms behind these NP-membrane interactions by calculating nanoscale parameters such as the number of extracted lipids, lipid diffusivity, and hydrophobic and hydrophilic interaction energy. We conclude that hydrophobic interaction is the most dominant driving force in all cases, while electrostatics also play a significant role in disrupting negative membranes when interacting with anisotropic NPs. This information is crucial in designing nanoparticles that can effectively target different lipid membranes.

By using metadynamics simulations, we demonstrated the preferred configuration of Janus NP when interacting with a lipid bilayer. This finding was then confirmed by comparing it with the behaviour of JP WM, revealing that uniform NP does not exhibit its preferred configuration when interacting with the membrane. These thermodynamics calculations shed light on the wrinkling effect induced by Janus NP. We presented various free energy surface calculations for different NP configurations and lipid compositions, which provide insights into the mechanism underlying NP-membrane interactions in terms of thermodynamics. More especially, we showcased that the anisotropic design of nanoparticles can help to disrupt the bacterial membrane. We demonstrated that JP 50/50 is able to extract the lipids and disrupt the bacterial membrane-mimicking model. This finding highlights the potential of using JP 50/50 design as an effective antimicrobial treatment. To validate our results, we compared the JP 50/50 design with uniform NP and found that the uniform NP did not have any disruptive effect on the bacterial membrane. Our study, by utilizing MD simulations, proposed that Janus NPs could effectively kill bacterial cells. Overall, this research offers promising insights into the development of new antimicrobial treatments through nanoparticle design.

Conflicts of interest

There are no conflicts to declare.

Acknowledgements

This work was mainly supported by the US National Science Foundation under grant numbers OAC-2326802 and CBET-2313754, as well as the associated Research Experiences for Undergraduates (REU) supplements. Support for this research was also provided by the University of Wisconsin–Madison, Office of the Vice Chancellor for Research and Graduate Education with funding from the Wisconsin Alumni Research Foundation.

References

1. C. Auria-Soro, T. Nesma, P. Juanes-Velasco, A. Landeira-Vinuela, H. Fidalgo-Gomez, V. Acebes-Fernandez, R. Gongora, M. J. Almendral Parra, R. Manzano-Roman and M. Fuentes, *Nanomaterials (Basel)*, 2019, **9**.
2. J. Chen, J. A. Hessler, K. Putchakayala, B. K. Panama, D. P. Khan, S. Hong, D. G. Mullen, S. C. Dimaggio, A. Som, G. N. Tew, A. N. Lopatin, J. R. Baker, M. M. Holl and B. G. Orr, *J Phys Chem B*, 2009, **113**, 11179-11185.
3. E. C. Cho, J. Xie, P. A. Wurm and Y. Xia, *Nano Letters*, 2009, **9**, 1080-1084.
4. R. R. Arvizo, O. R. Miranda, M. A. Thompson, C. M. Pabelick, R. Bhattacharya, J. D. Robertson, V. M. Rotello, Y. S. Prakash and P. Mukherjee, *Nano Lett*, 2010, **10**, 2543-2548.
5. O. Harush-Frenkel, E. Rozentur, S. Benita and Y. Altschuler, *Biomacromolecules*, 2008, **9**, 435-443.
6. A. Verma, O. Uzun, Y. Hu, Y. Hu, H. S. Han, N. Watson, S. Chen, D. J. Irvine and F. Stellacci, *Nat Mater*, 2008, **7**, 588-595.

7. R. C. Van Lehn, P. U. Atukorale, R. P. Carney, Y. S. Yang, F. Stellacci, D. J. Irvine and A. Alexander-Katz, *Nano Lett*, 2013, **13**, 4060-4067.
8. T. C. Le, J. Zhai, W. H. Chiu, P. A. Tran and N. Tran, *Int J Nanomedicine*, 2019, **14**, 6749-6777.
9. H. Su, C. A. Hurd Price, L. Jing, Q. Tian, J. Liu and K. Qian, *Mater Today Bio*, 2019, **4**, 100033.
10. C. Marschelke, A. Fery and A. Synytska, *Colloid and Polymer Science*, 2020, **298**, 841-865.
11. G. Agrawal and R. Agrawal, *ACS Applied Nano Materials*, 2019, **2**, 1738-1757.
12. H. Xie, Z. G. She, S. Wang, G. Sharma and J. W. Smith, *Langmuir*, 2012, **28**, 4459-4463.
13. K. Lee, L. Zhang, Y. Yi, X. Wang and Y. Yu, *ACS Nano*, 2018, **12**, 3646-3657.
14. K. Lee and Y. Yu, *Langmuir*, 2018, **34**, 12387-12393.
15. J. T. Wiemann, D. Nguyen, Y. Li and Y. Yu, *iScience*, 2022, **25**.
16. Y. Ma, K. Poole, J. Goyette and K. Gaus, *Front Immunol*, 2017, **8**, 1513.
17. K. Lee and Y. Yu, *Soft Matter*, 2019, **15**, 2373-2380.
18. J. T. Wiemann, Z. Shen, H. Ye, Y. Li and Y. Yu, *Nanoscale*, 2020, **12**, 20326-20336.
19. H. Ode, M. Nakashima, S. Kitamura, W. Sugiura and H. Sato, *Front Microbiol*, 2012, **3**, 258.
20. S. A. Hollingsworth and R. O. Dror, *Neuron*, 2018, **99**, 1129-1143.
21. D. W. Borhani and D. E. Shaw, *J Comput Aided Mol Des*, 2012, **26**, 15-26.
22. S. J. Marrink, H. J. Risselada, S. Yefimov, D. P. Tieleman and A. H. de Vries, *The Journal of Physical Chemistry B*, 2007, **111**, 7812-7824.
23. V. D. S. e. al, GROMACS 2020 Manual, DOI: 10.5281/zenodo.3562495).
24. J. Lin and A. Alexander-Katz, *ACS Nano*, 2013, **7**, 10799-10808.
25. S. Nangia and R. Sureshkumar, *Langmuir*, 2012, **28**, 17666-17671.
26. M. S. Jahan Sajib, P. Sarker, Y. Wei, X. Tao and T. Wei, *Langmuir*, 2020, **36**, 13356-13363.
27. J. Lin, L. Miao, G. Zhong, C. H. Lin, R. Dargazangy and A. Alexander-Katz, *Commun Biol*, 2020, **3**, 205.
28. S. J. Marrink and D. P. Tieleman, *Chem Soc Rev*, 2013, **42**, 6801-6822.
29. P. C. Hsu, D. Jefferies and S. Khalid, *J Phys Chem B*, 2016, **120**, 11170-11179.
30. J. A. Graham, J. W. Essex and S. Khalid, *J Chem Inf Model*, 2017, **57**, 650-656.
31. P. C. Hsu, B. M. H. Bruininks, D. Jefferies, P. Cesar Telles de Souza, J. Lee, D. S. Patel, S. J. Marrink, Y. Qi, S. Khalid and W. Im, *J Comput Chem*, 2017, **38**, 2354-2363.
32. J. Q. Lin, Y. G. Zheng, H. W. Zhang and Z. Chen, *Langmuir*, 2011, **27**, 8323-8332.
33. X. Chen, D. P. Tieleman and Q. Liang, *Nanoscale*, 2018, **10**, 2481-2491.
34. J. K. Sheavly, J. A. Pedersen and R. C. Van Lehn, *Nanoscale*, 2019, **11**, 2767-2778.
35. Y. Xia, H. S. Jang, Z. Shen, G. D. Bothun, Y. Li and M. P. Nieh, *Langmuir*, 2017, **33**, 5745-5751.
36. T. S. Carpenter, C. A. Lopez, C. Neale, C. Montour, H. I. Ingolfsson, F. Di Natale, F. C. Lightstone and S. Gnanakaran, *J Chem Theory Comput*, 2018, **14**, 6050-6062.
37. J. Lee, X. Cheng, J. M. Swails, M. S. Yeom, P. K. Eastman, J. A. Lemkul, S. Wei, J. Buckner, J. C. Jeong, Y. Qi, S. Jo, V. S. Pande, D. A. Case, C. L. Brooks, A. D. MacKerell, J. B. Klauda and W. Im, *Journal of Chemical Theory and Computation*, 2016, **12**, 405-413.
38. T. A. Wassenaar, H. I. Ingolfsson, R. A. Bockmann, D. P. Tieleman and S. J. Marrink, *J Chem Theory Comput*, 2015, **11**, 2144-2155.
39. G. Bussi and A. Laio, *Nature Reviews Physics*, 2020, **2**, 200-212.
40. S. Salassi, L. Caselli, J. Cardellini, E. Lavagna, C. Montis, D. Berti and G. Rossi, *J Chem Theory Comput*, 2021, **17**, 6597-6609.
41. S. Raniolo and V. Limongelli, *Nat Protoc*, 2020, **15**, 2837-2866.
42. J. L. Knight and C. L. Brooks III, *Journal of Computational Chemistry*, 2009, **30**, 1692-1700.
43. V. Spiwok, M. Kurecka and A. Krenek, *Front Mol Biosci*, 2022, **9**, 878133.
44. G. A. Tribello, M. Bonomi, D. Branduardi, C. Camilloni and G. Bussi, *Computer Physics Communications*, 2014, **185**, 604-613.
45. U. D. Plumed, METAD, https://www.plumed.org/doc-master/user-doc/html/_m_e_t_a_d.html, (accessed June 20, 2022).
46. W. Humphrey, A. Dalke and K. Schulten, *Journal of Molecular Graphics*, 1996, **14**, 33-38.
47. L. Li, X. Shi, X. Guo, H. Li and C. Xu, *Trends Biochem Sci*, 2014, **39**, 130-140.
48. K. Bohinc, M. Spadina, J. Rescic, N. Shimokawa and S. Spada, *J Chem Theory Comput*, 2022, **18**, 448-460.
49. L. H. Klausen, T. Fuhs and M. Dong, *Nat Commun*, 2016, **7**, 12447.
50. R. M. Epand and R. F. Epand, *Biochim Biophys Acta*, 2009, **1788**, 289-294.
51. H. Nikaido and T. Nakae, in *Advances in Microbial Physiology*, eds. A. H. Rose and J. G. Morris, Academic Press, 1980, vol. 20, pp. 163-250.
52. S. Chakraborty, M. Doktorova, T. R. Molugu, F. A. Heberle, H. L. Scott, B. Dzikovski, M. Nagao, L. R. Stingaciu, R. F. Standaert, F. N. Barrera, J. Katsaras, G. Khelashvili, M. F. Brown and R. Ashkar, *Proc Natl Acad Sci U S A*, 2020, **117**, 21896-21905.
53. R. J. Alsop, L. Toppozini, D. Marquardt, N. Kucerka, T. A. Harroun and M. C. Rheinstadter, *Biochim Biophys Acta*, 2015, **1848**, 805-812.
54. F. T. Doole, T. Kumarage, R. Ashkar and M. F. Brown, *J Membr Biol*, 2022, **255**, 385-405.
55. J. T. Wiemann, D. Nguyen, Y. Li and Y. Yu, *iScience*, 2022, **25**, 105525.
56. L. Wang, C. Hu and L. Shao, *Int J Nanomedicine*, 2017, **12**, 1227-1249.
57. A. Staroń and O. Długosz, *Journal of Environmental Science and Health, Part A*, 2021, **56**, 680-693.
58. M. J. Hajipour, K. M. Fromm, A. A. Ashkarran, D. J. d. Aberasturi, I. R. d. Larramendi, T. Rojo, V. Serpooshan, W. J. Parak and M. Mahmoudi, *Trends in Biotechnology*, 2013, **31**, 61-62.
59. Y. Tu, M. Lv, P. Xiu, T. Huynh, M. Zhang, M. Castelli, Z. Liu, Q. Huang, C. Fan, H. Fang and R. Zhou, *Nat Nanotechnol*, 2013, **8**, 594-601.
60. S. L. Regen, *JACS Au*, 2021, **1**, 3-7.

61. X. Jiang, Y. Sun, K. Yang, B. Yuan, T. Velkov, L. Wang and J. Li, *Comput Struct Biotechnol J*, 2021, **19**, 3885-3891.
62. H. Yamamura, T. Hagiwara, Y. Hayashi, K. Osawa, H. Kato, T. Katsu, K. Masuda, A. Sumino, H. Yamashita, R. Jinno, M. Abe and A. Miyagawa, *ACS Omega*, 2021, **6**, 31831-31842.
63. S. R. Herschede, H. Gneid, T. Dent, E. B. Jaeger, L. B. Lawson and N. Busschaert, *Org Biomol Chem*, 2021, **19**, 3838-3843.
64. E. S. Williams, H. Gneid, S. R. Marshall, M. J. Gonzalez, J. A. Mandelbaum and N. Busschaert, *Org Biomol Chem*, 2022, **20**, 5958-5966.
65. J. L. Dombach, J. L. J. Quintana, T. A. Nagy, C. Wan, A. L. Crooks, H. Yu, C. C. Su, E. W. Yu, J. Shen and C. S. Detweiler, *PLoS Pathog*, 2020, **16**, e1009119.